Supplementary Information (SI) for Journal of Materials Chemistry C.

Self-assembly of poly(ionic liquid) block copolymer based dielectrics on semiconductor formation and performance.

Supporting Information

Laura E. Dickson[1], Samantha Brixi[1], Chase L. Radford[2], Joseph G. Manion[1], Timothy L. Kelly[2] and Benoît H. Lessard[1,3]

1. Department of Chemical and Biological Engineering, University of Ottawa, 161 Louis Pasteur, Ottawa, Ontario K1N 6N5, Canada.
2. Department of Chemistry, University of Saskatchewan, Saskatoon, Saskatchewan S7N 5C9, Canada
3. School of Electrical Engineering and Computer Science, University of Ottawa, 800 King Edward Ave. Ottawa, Ontario K1N 6N5, Canada.

*Corresponding author: benoit.lessard@uottawa.ca

Table S1. Physical properties of poly(S)-*b*-poly(VBBI$^+$ [X$^-$]-*r*-PEGMA) block copolymers (X = TFSI$^-$, BF$_4^-$, or PF$_6^-$).

Polymer ID [a]	Anion	σ (S cm^{-2})	$\bar{M}_{n}^{b}$ $[kg\ mol^{-1}]$	Đ $[\bar{M}_w/\bar{M}_n]$	$F_{STY}{}^{c}$	$F_{CMS}{}^{c}$	$F_{PEGMA}{}^{c}$	$R_{CMS/PEGMA}{}^{d}$
S-*b*-(V25-*r*-P75)	TFSI$^-$	3.6×10^{-8}	28.0	1.07	0.95	0.02	0.03	0.64
	BF$_4^-$	-						
	PF$_6^-$	-						
S-*b*-(V50-*r*-P50)	TFSI$^-$	3.4×10^{-7}	35.9	1.23	0.67	0.18	0.15	1.27
	BF$_4^-$	7.9×10^{-8}						
	PF$_6^-$	4.1×10^{-9}						
S-*b*-(V75-*r*-P25)	TFSI$^-$	1.7×10^{-7}	31.4	1.12	0.74	0.20	0.06	3.17
	BF$_4^-$	1.2×10^{-8}						
	PF$_6^-$	5.8×10^{-11}						
S-*b*-(V100-*r*-P0)	TFSI$^-$	1.4×10^{-9}	39.6	1.17	0.70	0.30	-	-
	BF$_4^-$	4.6×10^{-9}						
	PF$_6^-$	7.4×10^{-11}						

[a] The polymer names are defined as S-*b*-(VX-*r*-PY) where X/Y = the target ratio of chloromethylstyrene (CMS) (converted to VBBI$^+$ after initial polymerization) versus poly(ethylene glycol) methyl ether methacrylate (PEGMA) used in the synthesis of the pre-polymer. The polymer synthesis and characterization data in this table are initially reported in Peltekoff *et al.*[41]

[b] The molecular weight of the polystyrene block is identical for all polymers, at 22.5 kg mol^{-1}.

[c] Molar composition of monomer unit determined by ^{1}H NMR. STY = styrene, CMS = chloromethyl styrene, PEGMA = poly(ethylyene glycol) methyl ether methacrylate.

[d] Ratio of CMS to PEGMA on a molar basis in the second block.

Table S2. Contact angle of deionized water on P(NDI2OD-T2) cast on quartz and diiodomethane on Si. Averages are presented plus/minus the standard deviation of 3 individual measurements.

Substrate	**Contact Angle (°)**
Si	93.62 ± 1.70
P(NDI2OD-T2) cast on quartz	46.00 ± 2.88

Table S3. PIL gating layer thickness and roughness determined by profilometry. Averages are presented plus/minus the standard deviation of 6 individual measurements.

Polymer	**Thickness (nm)**	**Roughness (nm)**
BF_4^-		
S-b-(V100-r-P0)	860.4 ± 57.4	62.7 ± 15.2
S-b-(V75-r-P25)	905.6 ± 44.0	52.3 ± 11.2
S-b-(V50-r-P50)	642.1 ± 101.8	37.9 ± 6.7
S-b-(V25-r-P75)	561.0 ± 77.3	38.5 ± 8.5
PF_6^-		
S-b-(V100-r-P0)	475.5 ± 69.2	89.2 ± 7.7
S-b-(V75-r-P25)	569.0 ± 69.0	29.9 ± 27.7
S-b-(V50-r-P50)	564.4 ± 41.5	39.2 ± 20.2
S-b-(V25-r-P75)	528.7 ± 50.2	52.2 ± 15.4
$TFSI^-$		
S-b-(V100-r-P0)	385.4 ± 44.1	25.6 ± 9.0
S-b-(V75-r-P25)	396.6 ± 37.9	23.1 ± 8.7
S-b-(V50-r-P50)	397.0 ± 34.4	45.0 ± 29.8
S-b-(V25-r-P75)	531.3 ± 65.2	22.9 ± 8.1

Table S4. Extracted d-spacing data from the azimuthally-integrated diffraction patterns at the three diffraction peaks, determined by GIWAXS.

Polymer	**d_{100} (Å)**	**d_{200} (Å)**	**d_{300} (Å)**	**d_{010} (Å)**
BF_4^-				
S-b-(V100-r-P0)	14.29	8.75	6.65	2.99
S-b-(V75-r-P25)	14.29	NA	6.83	3.00
S-b-(V50-r-P50)	14.29	NA	6.71	2.98
S-b-(V25-r-P75)	14.29	8.82	6.98	3.01
PF_6^-				
S-b-(V100-r-P0)	14.07	NA	6.83	2.99
S-b-(V75-r-P25)	14.29	NA	6.69	3.01
S-b-(V50-r-P50)	14.29	9.16	6.78	3.01
S-b-(V25-r-P75)	14.29	9.16	6.78	3.00
$TFSI^-$				
S-b-(V100-r-P0)	13.88	NA	6.79	3.02
S-b-(V75-r-P25)	14.07	9.24	6.69	3.01
S-b-(V50-r-P50)	13.88	9.06	6.69	3.03
S-b-(V25-r-P75)	14.07	9.16	6.79	3.02
F_{16}CuPc on Si				
-	14.07	9.24	6.88	3.06

Table S5. Full width half maxima of the (100) diffraction peak from the azimuthally integrated diffraction patterns determined by GIWAXS.

Polymer	**FWHM ($Å^{-1}$)**
BF_4^-	
S-b-(V100-r-P0)	0.052
S-b-(V75-r-P25)	0.052
S-b-(V50-r-P50)	0.046
S-b-(V25-r-P75)	0.052
PF_6^-	
S-b-(V100-r-P0)	0.052
S-b-(V75-r-P25)	0.052
S-b-(V50-r-P50)	0.052
S-b-(V25-r-P75)	0.052
$TFSI^-$	
S-b-(V100-r-P0)	0.059
S-b-(V75-r-P25)	0.078
S-b-(V50-r-P50)	0.078
S-b-(V25-r-P75)	0.046
$F_{16}CuPc$ on Si	
-	0.026

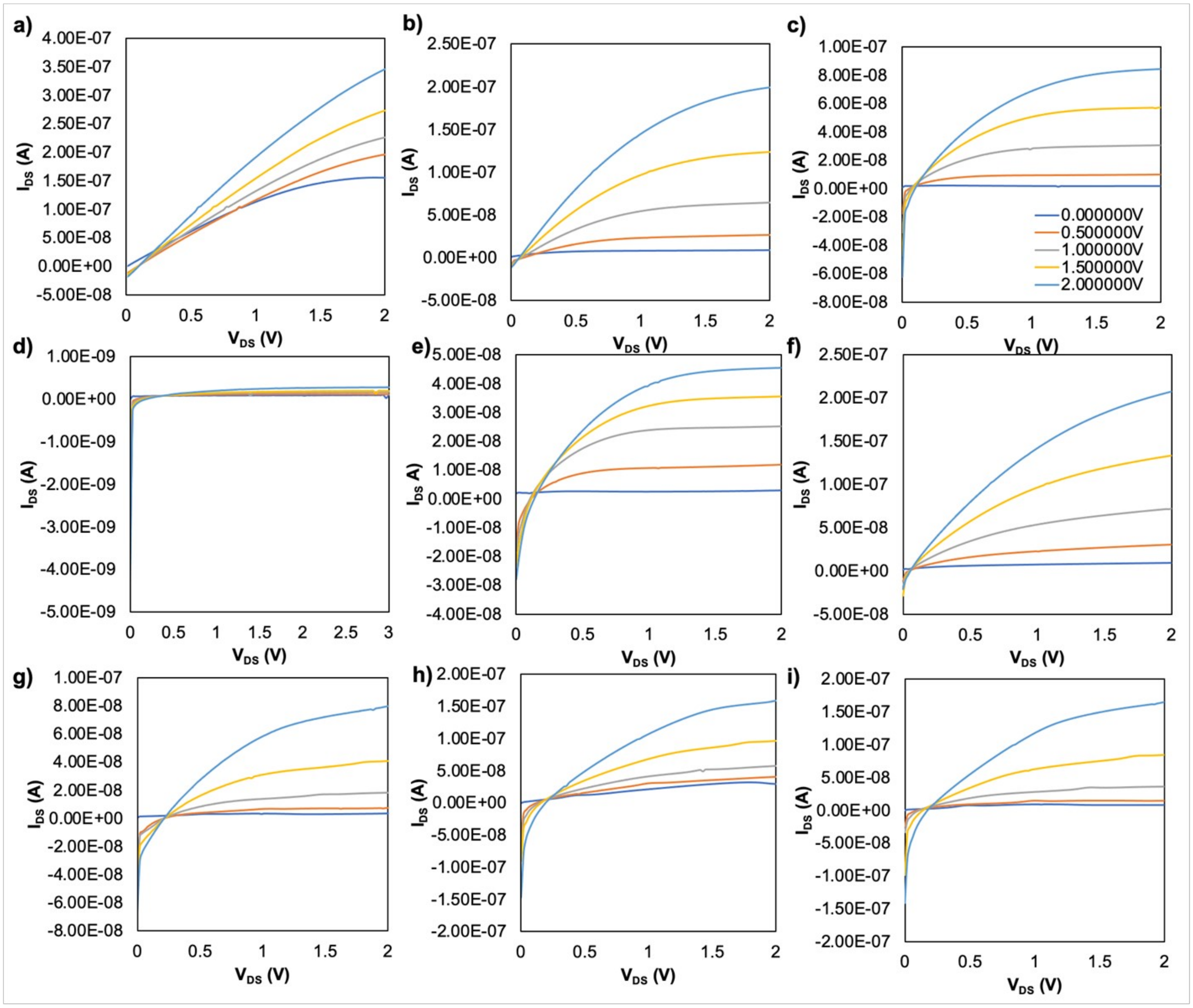

Figure S1. (a-c) Sample output curves for OTFT devices fabricated with $F_{16}CuPc$ on thin films of poly(S)-b-poly(VBBI+[PF_6^-]-r-PEGMA) block copolymers, with varying PEGMA/VBBI+ ratios of (a) S-b-(V100-r-P0), (b) S-b-(V75-r-P25), and (c) S-b-(V50-r-P50). (d-f) Sample output curves for OTFT devices fabricated with $F_{16}CuPc$ and thin films of poly(S)-b-poly(VBBI+[BF_4^-]-r-PEGMA) block copolymers, with varying PEGMA/VBBI+ ratios of (d) S-b-(V100-r-P0), (e) S-b-(V75-r-P25), and (f) S-b-(V50-r-P50). (g-i) Sample output curves for OTFT devices fabricated with $F_{16}CuPc$ and thin films of poly(S)-b-poly(VBBI+[TFSI$^-$]-r-PEGMA) block copolymers, with varying PEGMA/VBBI+ ratios of (g) S-b-(V100-r-P0), (h) S-b-(V75-r-P25), and (i) S-b-(V50-r-P50).

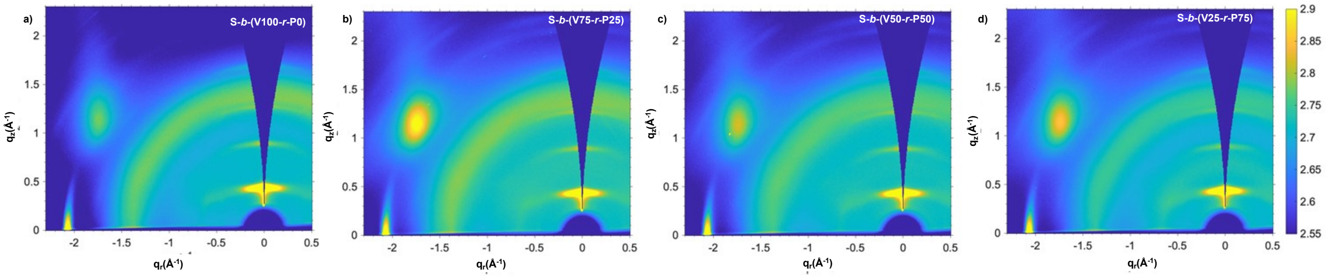

Figure S2. Grazing-incidence wide-angle X-ray scattering patterns of $F_{16}CuPc$ on PEGMA loading of (a) 0%, (b) 25%, (c) 50%, and (d) 75% for the PF_6^-.

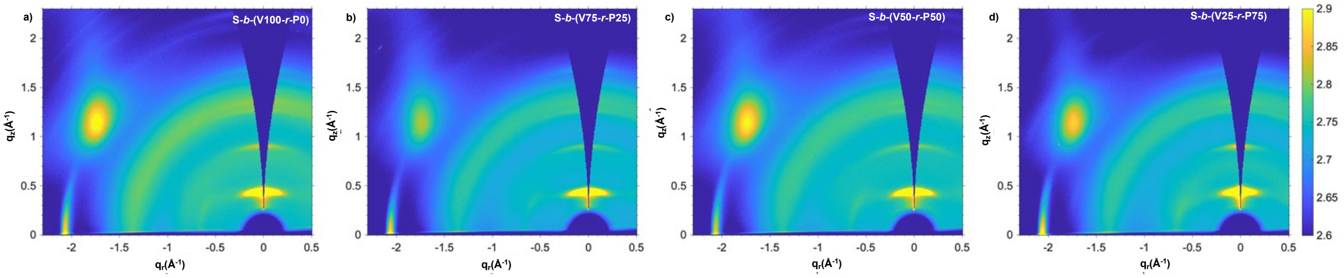

Figure S3. Grazing-incidence wide-angle X-ray scattering patterns of $F_{16}CuPc$ on PEGMA loading of (a) 0%, (b) 25%, (c) 50%, and (d) 75% for the $TFSI^-$.

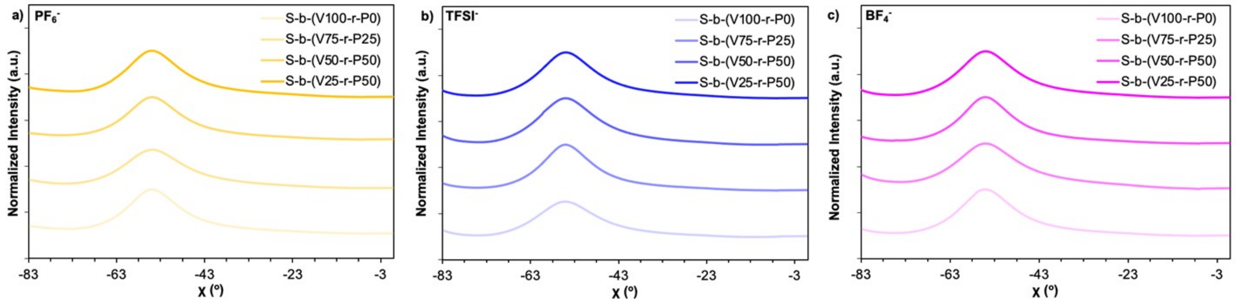

Figure S4. Pole figures for the (100) diffraction peak ($0.25\ Å^{-1} < q < 0.55\ Å^{-1}$) with Gaussian fits of $F_{16}CuPc$ on various PILs for (a) PF_6^-, (b) $TFSI^-$, and (c) BF_4^-.

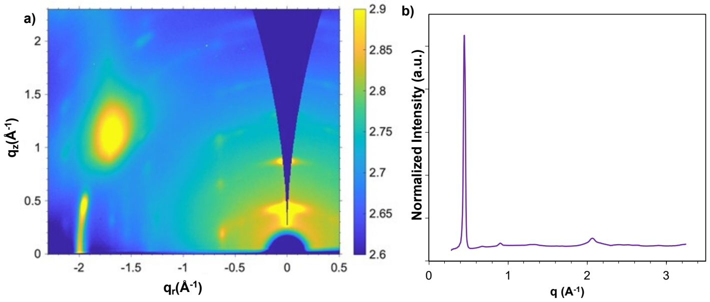

Figure S5. (a) 2D Grazing-incidence wide-angle X-ray scattering pattern and (b) azimuthally integrated linecut of F_{16}CuPc on Si. Integration occurs from $-83° < \chi < -1°$ and 0.12 Å$^{-1} < q < 2.3$ Å^{-1} to account for the Yoneda peak.

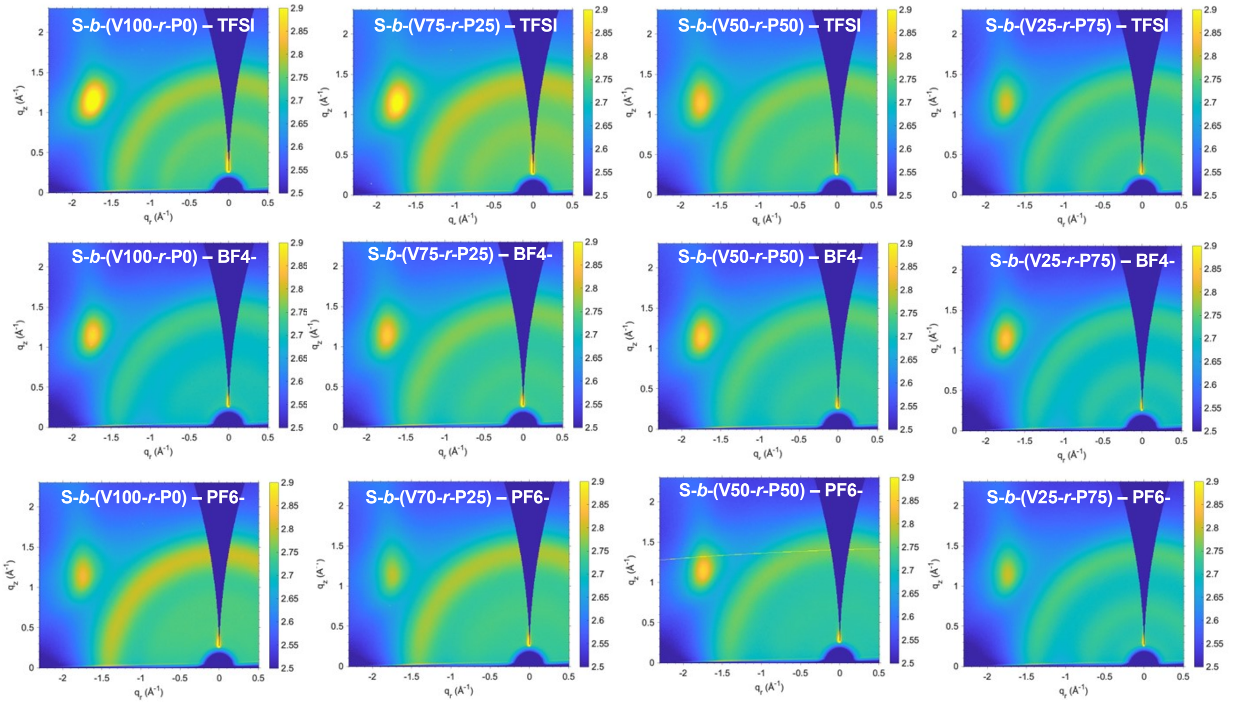

Figure S6. Grazing-incidence wide-angle X-ray scattering patterns of the PILs with different PEGMA/VBBI+ ratios and counterions.

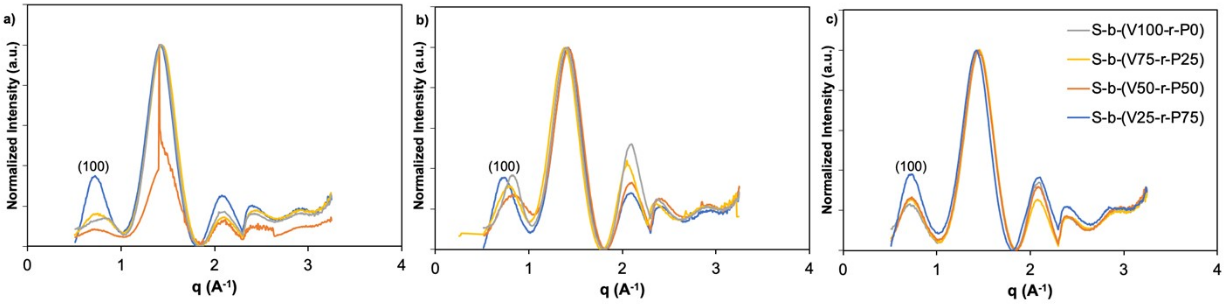

Figure S7. Grazing-incidence wide-angle X-ray azimuthally integrated diffraction patterns of the PILs with different PEGMA/VBBI+ ratios and the counterion (a) PF_6^-, (b) $TFSI^-$, and (c) BF_4^-. Integration occurs from $-83° < \chi < -1°$ and 0.12 Å$^{-1} < q < 2.3$ Å^{-1} to account for the Yoneda peak.

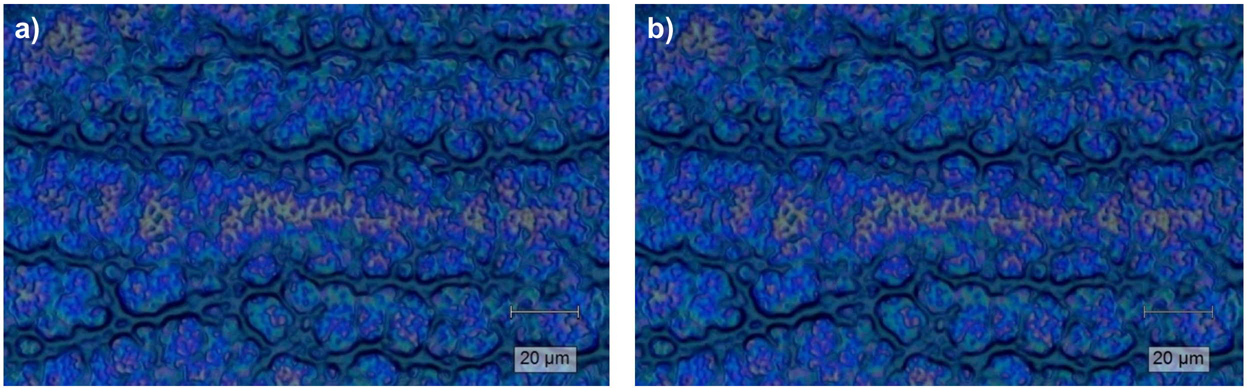

Figure S8. Sample microscopy image with x50L magnification of the sample map area before (a) and after (b) polarized maps were taken for S-*b*-(V75-*r*-P25) and the counterion PF_6^-.

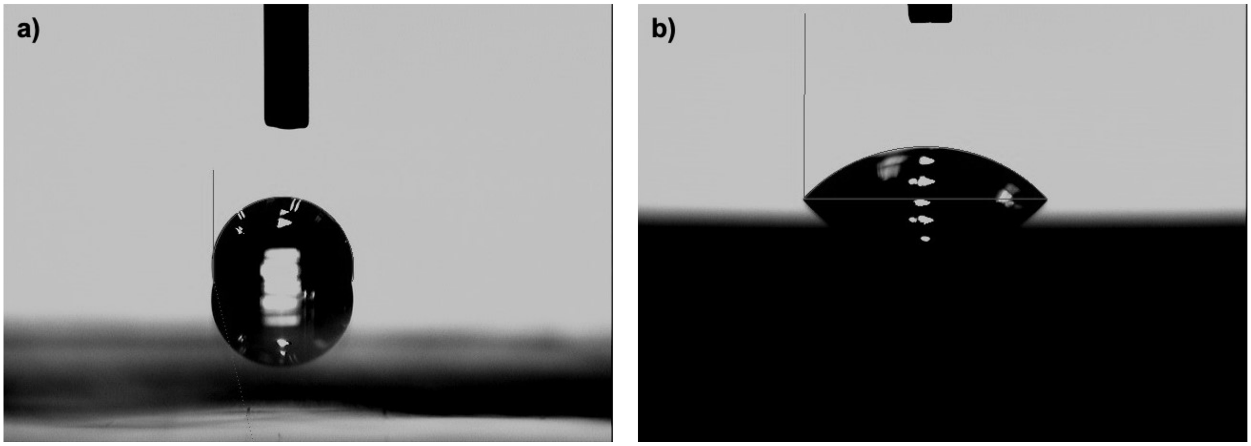

Figure S9. Sample contact angle images of (a) deionized water on P(NDI2OD-T2) cast on quartz and (b) diiodomethane on Si. Actual contact angle values are reported in **Table S2**.

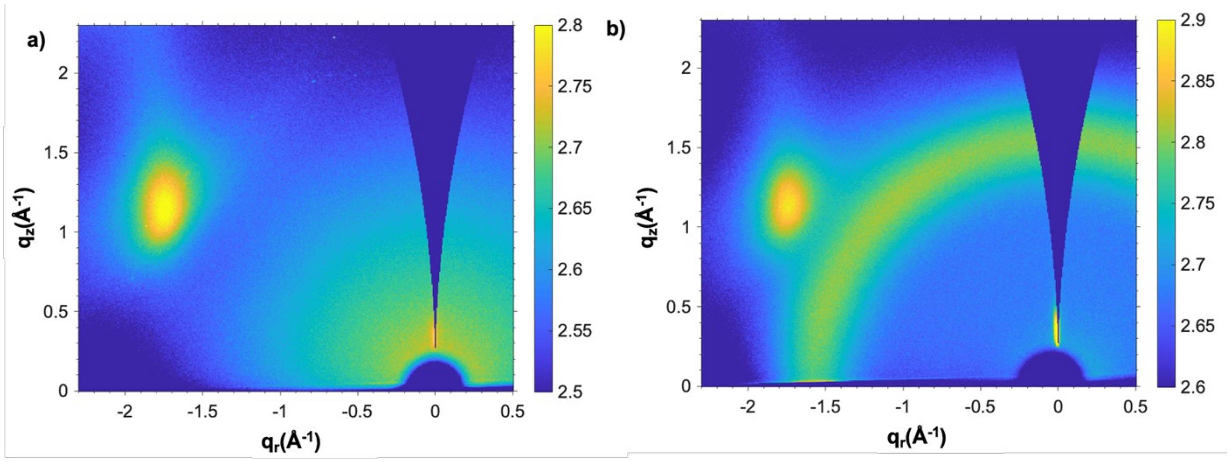

Figure S10. Grazing-incidence wide-angle X-ray scattering patterns of (a) pure Si and (b) SiO_2 thermally grown on Si.

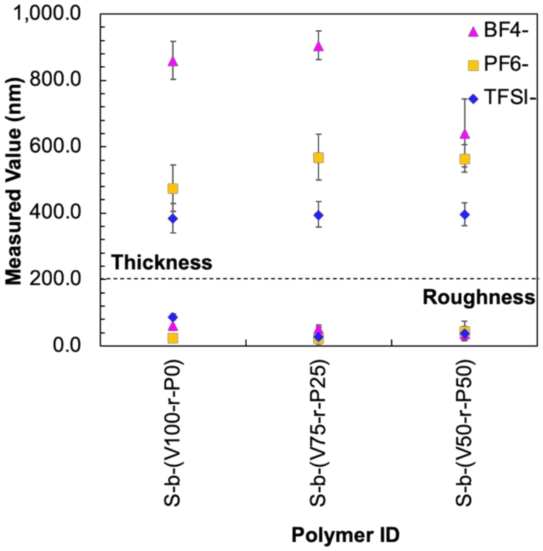

Figure S11. PIL gating layer thickness and roughness determined by profilometry (from **Table S3**).